Understanding structure, bonding and reactions of nanocrystalline semiconductors: novel high-resolution instrumental method of solid-state synchronous luminescence spectroscopy

Journal:	*Physical Chemistry Chemical Physics*
Manuscript ID	CP-PER-12-2020-006709.R1
Article Type:	Perspective
Date Submitted by the Author:	01-Mar-2021
Complete List of Authors:	Samokhvalov, Alexander; Morgan State University, Chemistry Department

Understanding structure, bonding and reactions of nanocrystalline semiconductors: novel high-resolution instrumental method of solid-state synchronous luminescence spectroscopy

Alexander Samokhvalov

Correspondence: Dr. Alexander Samokhvalov, Department of Chemistry, Morgan State University, 1700 East Cold Spring Lane, Baltimore, MD, 21251, USA.

E-mail: Alexandr.Samokhvalov@morgan.edu

Abstract

This Perspective Article describes recent advancements in studies of nanocrystalline metal oxides using novel ultra-high resolution method, solid-state synchronous luminescence spectroscopy (SS-SLS). Semiconductors notably include titanium dioxide and these studies shed light on detailed electronic structure, composition, and their reactions. First, we critically discuss limitations of major existing non-spectroscopic and spectroscopic methods of characterization of electronic structure of nanocrystalline semiconductors and insulators. Second, we describe the foundations and the setup of SS-SLS as an enhanced-resolution, facile, non-contact, non-destructive, and highly capable method of studies of nanomaterials. Third, the following insights are featured which are obtained by SS-SLS, but are not available by other methods: a) detection of traps of electric charge (specific mid-gap states); b) discrimination between "surface" and "bulk" sites; c) *in-situ* studies of composite nanomaterials and mechanisms of reactions, d) the derivative SS-SLS for accurate determination of energies of absorption and emission. The specific advantages of SS-SLS versus other methods and in direct comparison with "conventional" photoluminescence spectroscopy are highlighted. Finally, new opportunities and challenges of SS-SLS are presented. The SS-SLS is an advanced spectroscopic method with significant potential to aid academia and industry in studies in chemo-sensing, photocatalysis, optoelectronic materials, applied surface science, development of instrumental analysis, and studies of mechanisms of surface and "bulk" chemical reactions.

Keywords: semiconductor; synchronous luminescence spectroscopy; nanocrystal; surface; mid-gap state; adsorption

1) Introduction

Absorption and emission of light by solid-state nanomaterials reveal their optical and electronic structure and properties. Here, "optical properties" and "electronic properties" describe the similar items, and refer to absorption and emission of light by matter with concomitant excitation and relaxation of electrons. Absorption and emission allow to determine the structure of solids, since its change during reaction is accompanied by changes in electronic properties. Indeed, reactions are routinely monitored via changes in optical properties of reactants and/or products, which reflect changes in bonding.

Optical absorption, emission and the associated energy levels in solids are studied by several instrumental methods, notably including absorption and emission (luminescence) spectroscopy. Also, certain non-optical spectroscopic and non-spectroscopic methods are used. In determination of electronic structure of materials, photoluminescence (PL) spectroscopy and its varieties find significant interest. Unfortunately, the most solids and particularly solid-state nanomaterials yield very broad PL spectra, which do not allow detection of specific wavelengths (energies) of photons absorbed and emitted by the given material. This drawback is particularly severe at ambient and elevated temperatures, and the full widths at the half maxima (FWHMs) of spectral peaks commonly exceed 100 nm or even 200 nm. The solid-state synchronous luminescence spectroscopy (SS-SLS) offers unprecedented resolution and significant improvement in detection of several absorption/emission transitions in one experiment. Below, a brief review of electronic structure of solids is followed by critical assessment of existing spectroscopic and non-spectroscopic methods, and specific advantages of the SS-SLS.

2) Existing methods to study electronic structure of solids and absorption/emission of light

2.1) Basic electronic structure of solids: energy bands, mid-gap levels, and transitions

Semiconductors and insulators have a direct and/or indirect bandgap with energy E_g between the valence band VB (equivalent of the HOMO) and conduction band CB (equivalent of the LUMO). The E_g is defined as energy difference between the conduction band minimum (CBM) and valence band maximum (VBM), Figure 1. For direct bandgap materials, excitation of an electron from the VB to the CB occurs without lattice vibration, while for indirect bandgap the excitation of phonon is required.

Upon photoexcitation, photon emission proceeds from the CB to the VB and between the CB or VB and mid-gap states. Mid-gap states can be described as impurities and they are extensively studied by experiments [1] and simulations [2]. Mid-gap states are also termed "trapping states" since they attract and retain charge carriers (electrons or holes), or react with molecules as electron donors or acceptors. This drives significant attention to mid-gap states in semiconductor science and technology, opto-electronic materials e.g. photovoltaics [3], photocatalysis, sensing, and so on.

Mid-gap state are present in crystalline and amorphous nanomaterials [4] and are referred to as local defects, since they are distinctly different from delocalized energy bands. They are classified as intrinsic (in pure materials) and extrinsic, which are formed because of chemical reaction or physical impact (temperature, the ionizing radiation, etc.).

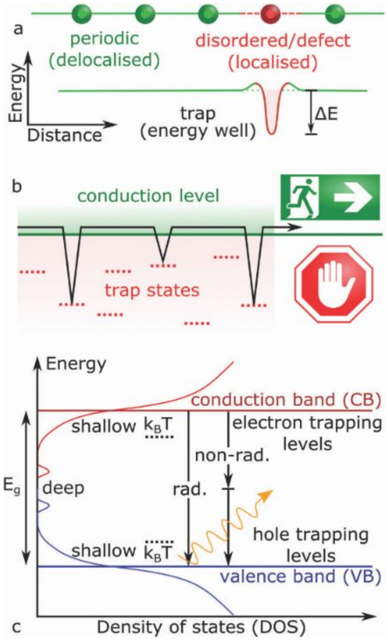

Figure 1. (a) Scheme of a charge localization caused by non-periodic disorder and defect in a semiconductor lattice (top), which introduce new energetic levels (bottom). (b) Scheme of charge trapping kinetics, where trap slow down charge carrier transport through trapping and detrapping events, as described by eqn (1). (c) Schematic representation of state density in a disordered semiconductor, whereby both band-to-band radiative (rad.) and non-band-to-band non-radiative (non-rad.) recombination (vertical arrows) can occur.
From Ref. [5]. H. Jin, E. Debroye, M. Keshavarz, I. G. Scheblykin, M. B. J. Roeffaers, J. Hofkens and J. A. Steele, It's a trap! On the nature of localised states and charge trapping in lead halide perovskites, *Mater. Horiz.*, 2020, 7, 397. Published by The Royal Society of Chemistry. This article is licensed under a Creative Commons Attribution-NonCommercial 3.0 Unported Licence.

In materials characterization, it is often desired to study the "entire" electronic structure: energy bands *and* mid-gap states. Advantages and limitations of pertinent instrumental methods are discussed below.

2.2) Non-optical spectroscopic, non-spectroscopic methods, and their combinations

Herein, the solid is probed by a) photon with energy much higher than that of transition of interest, b) an electron, or c) other particle such as neutron.

The ultraviolet photoemission spectroscopy, UPS

The UPS is conducted by illuminating the sample with a beam of photons of energy in the UV range ca. 0.5 - 100 eV. The photoelectrons are ejected from the VB and their energy E(VB) is determined. The UPS uses photons and as such can be considered optical method. However, in the context of this discussion, "optical" means optical range of spectrum, i.e. ca. 200-800 nm where the materials of interest absorb photons, across or within optical bandgap. Here, the UPS which mainly uses high energy ultraviolet photons, in most cases with energy well in excess of optical bandgap of most materials, and which generates free electrons (photoelectrons), is not classified as "optical spectroscopic method". To determine E(CB), inverse photoemission spectroscopy, IPES is used where beam of electrons with constant kinetic energy probes the sample. Hence, one has to combine the UPS and IPES to determine E_g for example for TiO_2 as in Figure 2.

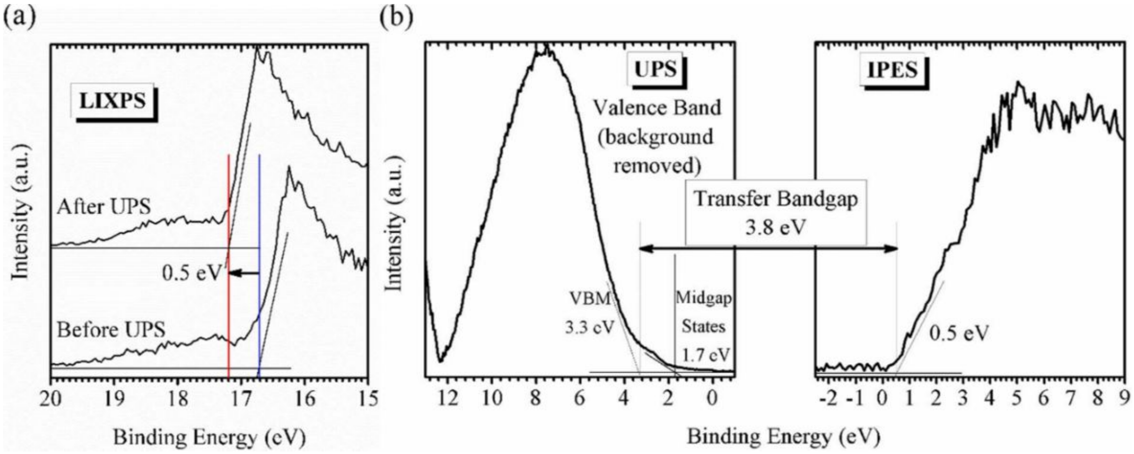

Figure 2. (a) Normalized secondary electron cutoff of low-intensity XP-spectra on a nanocrystalline TiO_2 thin-film before and after UPS measurements. Bottom spectra allow the determination of the WF before UV exposure. The shift of the secondary edge is due to the exposure to UV light during the UPS measurements which resulted in a WF reduction. (b) The combined UPS and IPES spectra of the TiO_2 nanoparticles. The left spectrum refers to the valence region measured, using UPS after background subtraction. The right spectrum represents the conduction band above the Fermi level, measured using IPES with 20 scans.

From Ref. [6]. H. Yaghoubi, Z. Li, Y. Chen, H.T. Ngo, V.R. Bhethanabotla, B. Joseph, S. Ma, R. Schlaf and A. Takshi, Toward a visible light-driven photocatalyst: The effect of midgap-states-induced energy gap of undoped TiO_2 nanoparticles, *ACS Catal.*, 2015, 5, 327-335. https://pubs.acs.org/doi/10.1021/cs501539q. Further permissions related to the material excerpted should be directed to the ACS.

Or, one can combine UPS and absorption spectroscopy as demonstrated by measurements of E_g in titanium dioxide nanopowder [7]. However, the UPS signal due to mid-gap states appears as a featureless edge (Figure 2b) and is poorly resolved so analysis of individual mid-gap states is not possible. Other combinations include scanning tunneling microscopy (STM) plus scanning tunneling spectroscopy (STS) e.g. to determine bandgap in 2D insulator molybdenum disulfide [8]. However, one needs to use high vacuum or the ultrahigh vacuum chambers since electrons are scattered in air. This creates challenges in studies of highly porous materials such as sorbents and catalysts which require a long time to “outgas” adsorbed air, water etc.

Electron energy loss spectroscopy EELS

In EELS, specimen is illuminated with electron beam of kinetic energy E_k and on impact, electrons transfer ΔE_k to excite transitions between the VB and CB, and the maximum signal is at $\Delta E_k = E_g$. EELS and reflection electron energy loss spectroscopy (REELS) were used to determine E_g in “simple” semiconductors e.g. titanium dioxide [9] and composite nanomaterials [10]. However, the energy resolution in EELS spectra is normally limited by about 1 eV, see Figure 3.

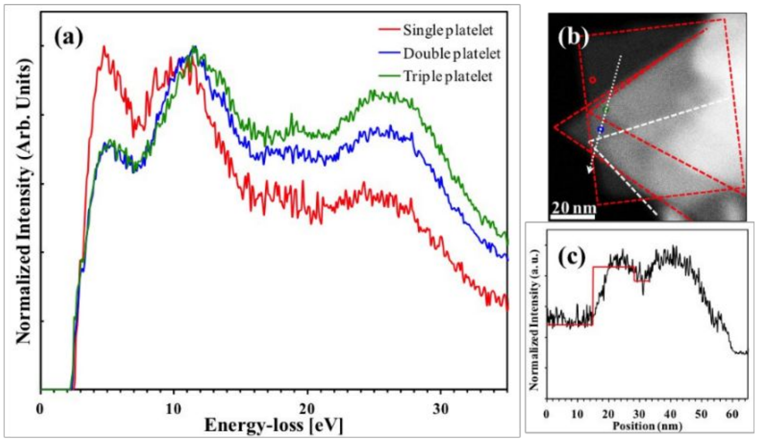

Figure 3. Valence electron energy-loss spectra (a) acquired from the stack of platelets shown in the ADF image in (b). The intensity profile in (c) was taken along the dotted line in (b), in the direction indicated by the arrow. The enhancement of the bulk feature with respect to the surface features occurs in agreement with the increment of thickness, given by the overlap between platelets. The spectra were acquired with a probe step of 4 nm, an energy resolution of 0.7 eV, a collection semi-angle of 4.5 mrad, an energy dispersion of 0.05 eV/pixel, and a dwell time of 1 s/pixel.

From Ref. [11]. Republished with permission of The Royal Society of Chemistry, from Probing the size dependence on the optical modes of anatase nanoplatelets using STEM-EELS, E. Liberti, R. Menzel, M.S.P. Shaffer and D.W. McComb, *Nanoscale*, vol. 8, pp. 9727-9735, Copyright 2016. Permission conveyed through Copyright Clearance Center, Inc. Order license ID1087055-1.

Resolution of EELS is often not sufficient to resolve individual mid-gap states, and significant efforts are needed to improve resolution [12] to 0.2-0.3 eV. Only very recently, using sophisticated apparatus allowed improvement of resolution down to millielectron volts [13]. The more common approach is to combine EELS with scanning transmission electron microscope via STEM-EELS [14], or scanning electron microscope via SEM-EELS [15]. Unfortunately, radiation damage is common in EELS, TEM-EELS and STEM-EELS [16] and mid-gap surface states are particularly sensitive to it. Another obvious drawback is the need of the sophisticated instruments.

Neutron scattering

This is non-spectroscopic technique of nanomaterials characterization [17] and there are reports on determination of E_g in semiconductors by neutron scattering [18]. However, this is an indirect approach which has limitations. First, as any scattering technique, neutron scattering is most useful in determination of atomic arrangement, rather than electronic transitions. We are not aware of studies of mid-gap states in semiconductors by neutron scattering. Second, one needs access to an off-campus facility such as a national research lab.

2.3) The UV-Visible diffuse reflectance spectroscopy, UV-Vis DRS

The UV-Vis DRS is the most common method to learn about absorption of light in solids and changes in optical properties. In the literature, it is common to use absorbance aka absorption spectra to present the data collected by UV-Vis spectrometer with diffuse reflectance (DR) accessory and with light reflected from solid-state sample upon absorption. In nanocrystalline semiconductors and insulators, the energy E_g of optical transition across the bandgap is determined by processing the UV-Vis DR spectra; an example [19] is in Figure 4. Inset of Figure 4 shows a "defect related hump" due to light absorbing mid-gap states, aka the Urbach tail which is explained below.

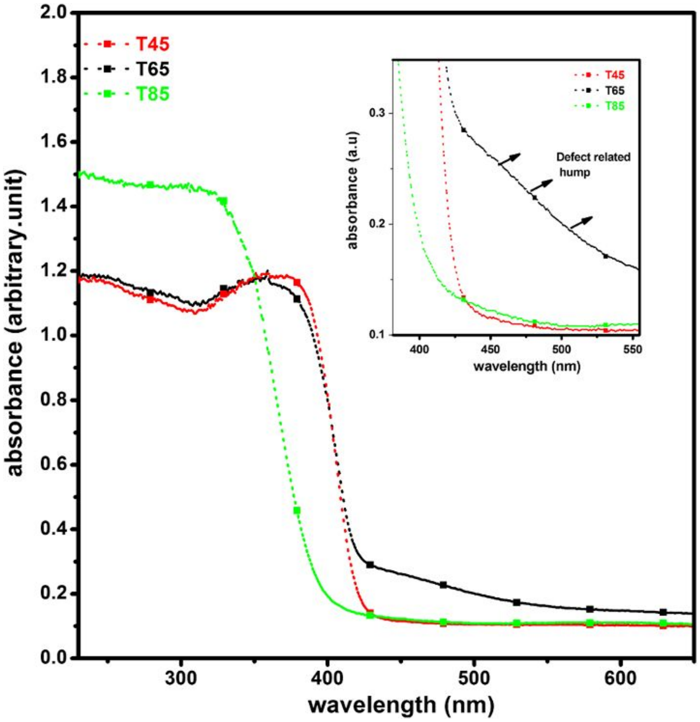

Figure 4. UV–Vis absorption study annealed at different temperatures.
From Ref. [19]. S. Paul, A. Choudhury, Investigation of the optical property and photocatalytic activity of mixed phase nanocrystalline titania, *Appl. Nanosci.*, 4 (2014) 839-847.
This is an open access article distributed under the terms of the Creative Commons CC BY license, which permits unrestricted use, distribution, and reproduction in any medium, provided the original work is properly cited.

Often, UV-Vis DRS can be represented through Kubelka-Munk (KM) function describing optical absorbance corrected for scattering. It is $F(R) = (1 - R)^2/2R = k/s$ where k is the KM absorption coefficient and s is optical scattering constant [20]. Or, E_g is determined from the Tauc plot $(\alpha\ E)^{1/n} = E - E_g$ where E is photon energy, α is absorption coefficient, and n is Tauc constant [21]. The Tauc plot and F(R) function can be combined [22] resulting in $(F(R)\ E)^{1/n} = E - E_g$. For direct bandgap materials n = ½ while for an indirect bandgap n = 2.

In Figure 5, bandgap of TiO_2 nanoparticles is calculated from the extrapolated "blue edge". The extrapolation procedure results in error; the bigger disadvantage of UV-Vis DRS is lack of information about transitions other than the bandgap. First, they include the extrabandgap transitions with $E>E_g$ since these peaks are very wide and obscured by the bandgap transition. Second, UV-Vis DRS is very limited in analysis of individual subbandgap transitions at $E<E_g$ which form the Urbach edge [23].

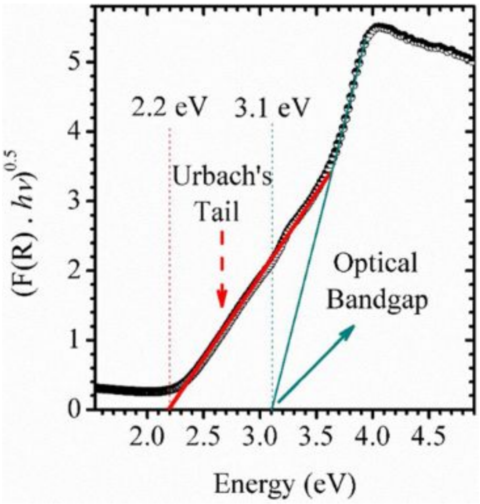

Figure 5. Plot of transformed Kubelka−Munk function vs the energy of the excitation source absorbed. The optical bandgap (narrow green line) and the Urbach tail (bold red line) are shown. From Ref. [6]. H. Yaghoubi, Z. Li, Y. Chen, H.T. Ngo, V.R. Bhethanabotla, B. Joseph, S. Ma, R. Schlaf and A. Takshi, Toward a visible light-driven photocatalyst: The effect of midgap-states-induced energy gap of undoped TiO_2 nanoparticles, *ACS Catal.*, 2015, 5, 327-335. https://pubs.acs.org/doi/10.1021/cs501539q. Further permissions related to the material excerpted should be directed to the ACS.

The Urbach tail is of interest in studies of major nanocrystalline semiconductors titanium dioxide [24], silicon [25], gallium nitride [26], and midgap states affect performance of optoelectronic e.g. photovoltaic nanomaterials [27] and photocatalysts [28]. Other limitations of UV-Vis DRS are large full widths at the half maxima (FWHMs) of peaks due to mid-gap states, and low sensitivity of detector in the spectrophotometer.

2.4) “Conventional” photoluminescence (PL) spectroscopy

In “conventional” PL or fluorescence *emission* spectroscopy, the photoexcitation wavelength λ_{exc} is constant, while photoemission wavelength λ_{emiss} is scanned producing emission spectrum. In the complementary excitation spectroscopy, the desired λ_{emiss} is kept constant while λ_{exc} is varied forming the excitation spectrum. The term “PL spectroscopy” is used when the lifetime of the photoexcited charge is unknown, while “fluorescence spectroscopy” means the lifetime from picoseconds to nanoseconds. Optical emission spectrometer (fluorimeter) is available in virtually every chemistry or materials science lab, this experiment can be facilely conducted under ambient conditions, and it is applicable to broad range of nanocrystalline materials.

For decades, “conventional” PL spectroscopy was used in analysis of solids, and it remains major tool for characterization of insulators and semiconductors of major interest [29] including microcrystalline and porous silicon [30]. More recent reports cover pure and doped nanocrystalline silicon [31], other semiconductors and semiconductor arrays [32]. Unfortunately, “conventional” PL spectra are usually quite wide and featureless, especially at ambient and elevated temperatures. Peaks due to specific transitions are strongly overlapped and their interpretation is tentative. This is illustrated by Figure 6 with “conventional” PL spectra of TiO_2 nanorods [33].

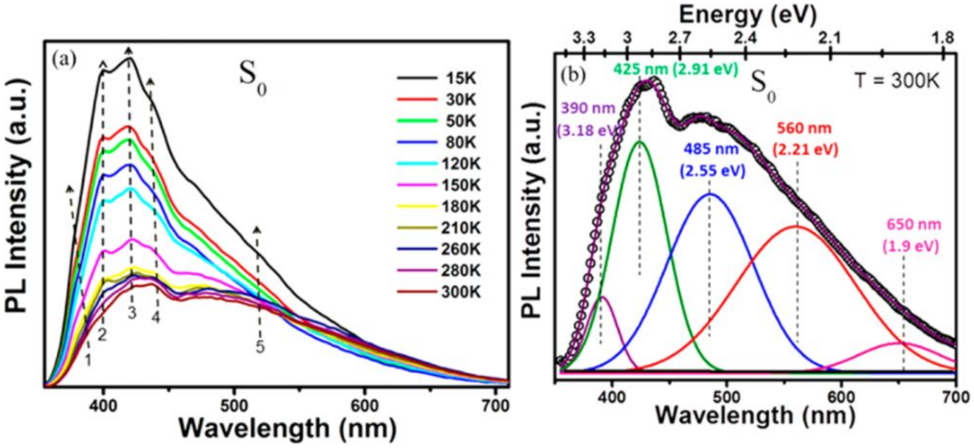

Figure 6. (a) Typical PL spectra of TiO_2 NRs on Si pyramids (i.e., S_0) in the temperature range of 15−300 K where the upward arrows indicate the existence of various defect-related emissions. The PL spectrum at 300 K is deconvoluted in (b), where the fitting components (marked by dashed lines) and the cumulative fitting profile (solid curve) are superimposed on the experimental data for clarity. The corresponding energy scale is also shown in the top abscissa. From Ref. [33]. Reprinted with permission from C.P. Saini, A. Barman, D. Banerjee, O. Grynko, S. Prucnal, M. Gupta, D.M. Phase, A.K. Sinha, D. Kanjilal, W. Skorupa and A. Kanjilal, Impact of self-trapped excitons on blue photoluminescence in TiO_2 nanorods on chemically etched Si pyramids, *J. Phys. Chem. C*, 2017, 121, 11448-11454. Copyright (2017) American Chemical Society.

In Figure 6b, spectral band measured at 300 K is de-convoluted into as many as *five* distinct peaks by multi-peak curve fitting. While some fitted components are plausible, others may be hard to observe and justify. Figure 6a illustrates the limitations of using cryo-temperature in "conventional" PL spectroscopy: while signal increases drastically, the resolution is barely improved.

The PL spectroscopy is of significant interest for characterization of broad bandgap semiconductors and insulators, notably including diamond which is used, for example, in micro/nano-electromechanical systems [34]. Further, "conventional" PL spectroscopy can be accomplished in several advanced variants, such as circularly polarized luminescence (CPL) [35]. However, they have the same limitations due to wide featureless spectra, especially at room and the elevated temperatures.

It is desired to review how the novel method of solid-state synchronous luminescence spectroscopy, SS-SLS aids in studies of semiconductors. This is convenient to start with the benchmark nanocrystaline semiconductors of simple composition "metal+oxygen" and specifically titanium dioxide.

3) The SS-SLS. Experimental setup

Optical setup for the SS-SLS experiment is an adaptation of geometry common for "conventional" PL and fluorescence spectra of concentrated solutions and solids [36]. However, it is important to briefly review the basics. In the overwhelming majority of studies of diluted solutions (ca $<1x10^{-3}$ mol/liter), the right-angle (RA) geometry is used, Scheme 1a. Such solution in the standard or reduced-volume cuvette of 1 mm – 10 mm thick absorbs very small fraction of incident light. Even for thicker specialty cuvettes up to few cm, absorption is low for both incident and emitted light across the UV, visible and near-infrared (NIR) range, due to the typical numeric values of molar extinction coefficient ε(λ) in the Beer law.

However, the RA geometry in studies of concentrated solutions and solids results in severe artifacts in spectra [37]. One common artifact is an increase of emission wavelength aka "red-shift artifact", and another is a decrease of signal intensity, which makes analysis of spectra difficult. These artifacts originate in re-absorption of emitted fluorescence, aka the inner-filter effect IFE [38].

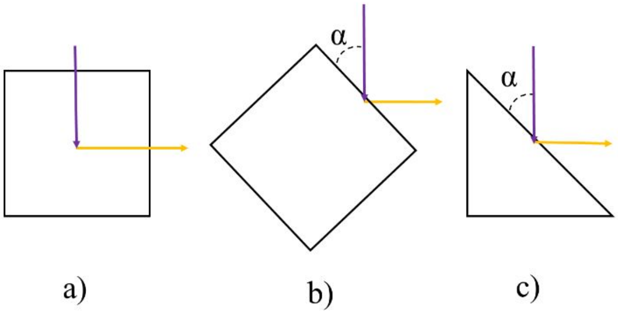

Scheme 1. Typical optical geometries in optical emission spectroscopy. a) The right angle (RA) for diluted solutions. The front-face (FF) with: b) standard cuvette; c) triangular cuvette.

To minimize IFE, the front-face (FF) geometry, Scheme 1b and 1c has been developed using the standard 3.7 cc cuvette made of quartz or Suprasil. Triangular cuvettes (Scheme 1c) are commercially available e.g. from Hellma Analytics, but seldom used. In the FF geometry, both excitation and emission light penetrate very short distance through the sample thus minimizing IFE [39]. The excitation beam is usually directed at 30 to 60 deg. to the front surface of cuvette; the 45 deg. is not recommended [36]. Most commercial fluorimeters have manual knob for facile change from the RA to the FF mode. The FF fluorescence finds a widespread use in diverse applications from analysis of liquids including water [40] to semi-solid matter e.g. food [41].

The SS-SLS experiment requires the FF geometry, and in it both λ_{exc} and λ_{emiss} are simultaneously ("synchronously") varied at a constant difference $\Delta\lambda$; this is referred to as constant wavelength (CW) synchronous fluorescence spectroscopy. The software packages of commercial fluorimeters contain built-in routines for collection of synchronous luminescence spectra in the CW mode. Authors of this paper have utilized the built-in software capabilities of several instruments. At one end, it is basic fluorimeter Cary Eclipse with a single monochromator on the excitation and emission paths. On the opposite end, it is a research-grade instrument Fluorolog3-22 from HORIBA Scientific with dual monochromators on both paths.

The SS-SLS experiment is straightforward even for novice researcher with some background in fluorescence spectroscopy. The capabilities and advantages of SS-SLS in studies of solid-state nanomaterials are explained below.

4) Capabilities of SS-SLS in characterization of semiconductors

4.1) Detection of charge trapping midgap states

Understanding charge-trapping states is of importance to industry of semiconductor devices [42]. In most semiconductors, there are several different mid-gap states which are intrinsic (present in pure material) or extrinsic (due to impurities). Mid-gap states can be located inside the nanocrystal or on surface. Hence, the energy of *specific* midgap state is difficult to determine, since many different states may contribute to the peak of interest. As noted above, peaks in "conventional" PL spectra of semiconductors are usually broad, featureless, and cannot be satisfactorily resolved into contributions from the individual midgap states of similar energy, and referenced to the CB, VB, or the vacuum level [43]. One example is mid-gap states above the Fermi level which are not populated with electrons [44], but can be transiently populated upon absorption of photon.

Alkaline earth metal titanates $MTiO_3$ (M = Mg, Ca, Sr, Ba) are the broad bandgap semiconductors of significant interest to science and technology. They find use in electronic devices [45], solid-state chemo-sensors [46], superconductors [47] and as sorbents [48], catalysts [49] and photocatalysts [50]. Specifically, in photocatalytic hydrogen generation it is important that the conduction band minimum (CBM) of a photocatalyst is at higher energy [51] (more negative electrode potential) than the CBM of the benchmark photocatalyst TiO_2. Amongst alkaline earth metal titanates, calcium titanate $CaTiO_3$ has the most negative CBM potential, and it was studied for photocatalytic hydrogen generation by several groups worldwide: in Japan [52], China [53], U.S. [54], Brazil [55] and covered in the review [56].

In 2016, our group pioneered [57] the SS-SLS studies of electronic structure of nanocrystalline inorganic semiconductors, Table 1.

Table 1. The SS-SLS studies of absorption and emission of light in nanocrystalline semiconductors

Material	Physical properties	Band gap and mid-gap states involved / / wavelength of transition, nm	Ref.
calcium titanate $CaTiO_3$	nanopowder, 100 nm, surface area 6.7 m^2/g	mid-gap state below CBM / 400 nm; STE* / 470 nm; exciton–like mid-gap state / 520 nm	57
calcium titanate $CaTiO_3$	mesoporous powder, surface area 10.4 m^2/g, pore volume 0.023 cm^3/g	only subbandgap transitions / excitation 420 nm; emission 440 nm, 465 nm, 490 nm	58
strontium titanate $SrTiO_3$	nanopowder, 100 nm	from mid-gap state below CBM / 430 nm; to mid-gap state / 460 nm; between mid-gap states / 500 nm	59
rutile TiO_2	nanopowder, 30 nm, surface area 50 m^2/g	bandgap / 413 nm; free exciton / 430 nm; mid-gap states / 520 nm, 560 nm	60
anatase TiO_2	nanopowder, 15 nm	mid-gap states / 420 nm, 450 nm; STE / 500 nm	61

* STE = strongly trapped exciton

To achieve a cryo-temperature of 77 K, a quartz cuvette filled with $CaTiO_3$ nanopowder was immersed into a mini-Dewar with liquid nitrogen (LN_2). An optically transparent, low-cost mini-Dewar is located directly in the sample compartment [57] of spectrometer Fluorolog3-22. The SS-SLS peaks are substantially narrower and better resolved [57] than peaks in "conventional" PL spectra at 77 K, Figure 7. The "R" is a Raman artifact due to LN_2 in a mini-Dewar.

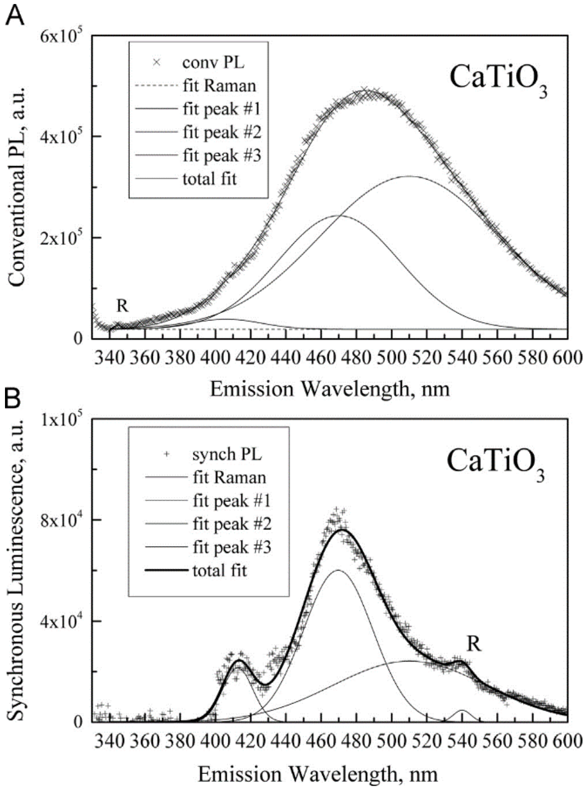

Figure 7. PL spectra of nanocrystalline $CaTiO_3$ at 77 K with Gaussian fitting. A) ”Conventional” PL spectrum at $\lambda_{exc} = 320$ nm. B) Synchronous luminescence spectrum at $\Delta\lambda = 60$ nm.
From Ref. [57]. Reprinted from *Journal of Luminescence*, Vol. 178, Azzah Alzahrani and Alexander Samokhvalov, “Conventional and cryo-synchronous luminescence spectra of orthorhombic calcium titanate”, pages 430–436, Copyright (2016), with permission from Elsevier. License Number 4977830876089.

Namely, “conventional” PL spectrum (Figure 7a) contains one very broad band with FWHM ca. 150 nm, which permits no conclusion about specific optical transitions excited in experiment. Further, Raman peak of LN_2 is a shoulder of the PL spectrum, along with other shoulders due to transitions, which compromises multi-peak fitting. In contrast, the SS-SLS (Figure 7b) shows the significant peak narrowing, with two clear peaks and a well-defined Raman artifact. The energy of each peak was successfully determined by fitting with a multi-Gaussian function. Peak assignments include three individual mid-gap states as in the energy diagram of transitions “absorption/emission” in $CaTiO_3$ in Scheme 2.

Importantly, transitions in $CaTiO_3$ have been excited by photons with energy higher *and* lower than E_g which are commonly referred to as extrabandgap $E \geq E_g$ and the subbandgap transitions $E \leq E_g$, respectively. The exciton in $CaTiO_3$ is quantum quasi-particle – the delocalized electron-hole pair, and it is interpreted as intrinsic mid-gap state.

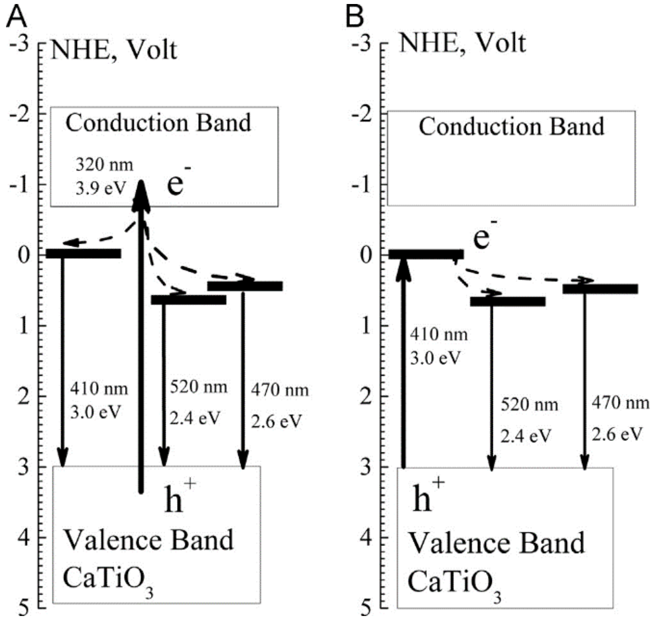

Scheme 2. Energy diagram of relaxation of photoexcited charge in the nanocrystalline $CaTiO_3$. A) At the extrabandgap excitation at 320 nm. B) At the subbandgap excitation at 410 nm.
From Ref. [57]. Reprinted from *Journal of Luminescence*, Vol. 178, Azzah Alzahrani and Alexander Samokhvalov, "Conventional and cryo-synchronous luminescence spectra of orthorhombic calcium titanate", pages 430–436, Copyright (2016), with permission from Elsevier. License Number 4977830876089.

The SS-SLS of $CaTiO_3$ in Ref. [57] was conducted at 77 K because this material has very weak luminescence at 25 °C. Further, Alzahrani et al. reported porous hierarchically meso/micro structured $CaTiO_3$ prepared with organic structure-building template [58] which shows strong visible luminescence at 25 °C due to lattice defects (extrinsic mid-gap states), including oxygen vacancies. Again, its SS-SLS are much better resolved [58] than "conventional" PL spectra, which allows assignments of the subbandgap transitions (Table 1). This is likely that the extrabandgap transitions occur on a very short time scale so they are not observed in the steady-state SS-SLS. Taylor et al. [59] reported that the SS-SLS of nanocrystalline strontium titanate $SrTiO_3$ at 25 °C reveal both excitation and emission transitions due to specific mid-gap states.

Alkaline earth metal titanates are composite semiconductors, as they contain two metal cations. The energy level diagrams of semiconductors of simpler composition e.g. titanium dioxide TiO_2 have been reported by SS-SLS. Specifically, charge-trapping mid-gap states have been identified by the SS-SLS in anatase [61] and rutile [60] nanopowder. Simpler composition allows more detailed studies as described below.

4.2) Accurate determination of energies of absorption and emission: derivative SS-SLS

In numeric analysis of "conventional" PL spectra, peak maximum is the highest intensity of emission function I(emiss) at the respective maximum emission wavelength λ_{emiss}. At peak maximum, the derivative dI(emiss) / dλ_{emiss} is zero. The so obtained "derivative conventional PL spectra" plotted as dI(emiss) / dλ_{emiss} versus λ_{emiss} are significantly narrower and better resolved than PL spectra [62], and yield better accuracy of λ_{emiss} and E_{emiss} energies than the PL spectra. This approach is commonly used in the 1-st derivative spectroscopic analysis of "conventional" luminescence [62], fluorescence [63], and phosphorescence [64] spectra.

In turn, the derivative SLS spectra can be plotted as dS(emiss$_{)}$ / dλ_{emiss} where S(emiss) is the maximum intensity of synchronous signal. The derivative SS-SLS offers a "double advantage" vs. "conventional" PL spectra: a) due to synchronous scanning and b) signal narrowing by digital derivative. Indeed, multiple studies in aqueous and non-aqueous solutions highlight specific advantages of derivative SLS: the significantly improved resolution of minor features, an enhanced selectivity of detection of multiple fluorophores in the same sample, the improved correction for background [65], and substantial lowering of detection limit. One would expect, that the derivative SLS is applied to studies of absorption and emission of light in solid-state nanomaterials; such studies were pioneered in 2017.

In photocatalysis and photovoltaics [66], it is important to know the accurate values of energies of absorption and emission. Titanium dioxide (titania) TiO_2 is the benchmark photocatalyst still of significant interest, which is extensively studied by spectroscopic methods [67]. To improve photocatalytic performance, anatase is doped with non-metals [68], metals [69], combinations "metal/metal" [70], "non-metal/non-metal" [71], "metal/non-metal" [72], and "defect engineered" e.g. by chemical reduction [73]. These synthetic routes result in new charge-trapping mid-gap states which can decrease or increase photocatalytic yield. Mid-gap states in anatase include "bulk" oxygen vacancies [74], surface oxygen vacancies [75], and self-trapped exciton (STE). The STE in anatase was reported for single crystals and films [76], nanorods [33] and nanoparticles [77]. Usually, STE is studied by "conventional" PL spectroscopy at cryo-temperatures when it has strong visible emission. Studies of STE using PL spectra at room temperature are difficult, due to weak emission and strong interference with other light-emitting mid-gap states.

Recently, we utilized the 1-st derivative SS-SLS [61] for accurate determination of energy of both absorption and emission of light by STE in nanocrystalline anatase at 25 °C. The STE is photoexcited *indirectly* by a photon of the extrabandgap energy (Scheme 3a) or directly at the subbandgap energy (Scheme 3b).

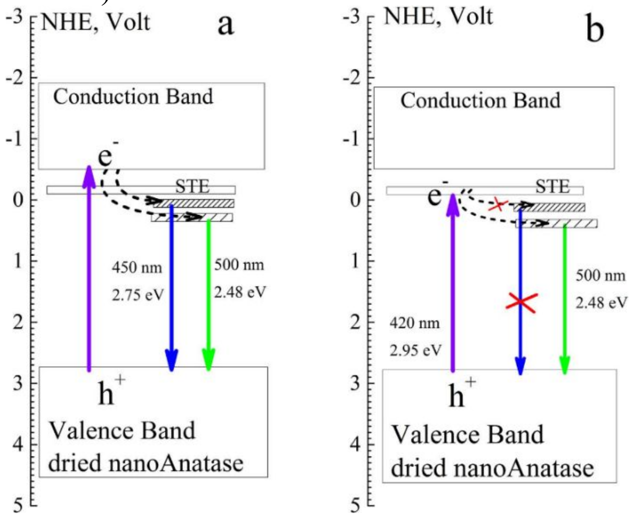

Scheme 3. The energy level diagram of transitions in dried nanocrystalline anatase. a) Extrabandgap photoexcitation. b) Subbandgap photoexcitation.

From Ref. [61]. Reprinted from *Journal of Luminescence,* Vol 192, Alexander Samokhvalov, Trap emission by nanocrystalline anatase in visible range studied by conventional and synchronous luminescence spectroscopy: Adsorption and desorption of water vapor, pages 388-396, Copyright (2017), with permission from Elsevier. License Number 4978280875192.

Direct photoexcitation allows much more accurate value of excitation energy E(STE) via determination of its absorption wavelength λ(STE). This requires an enhanced spectroscopic resolution, which is one of major advantages of derivative SS-SLS. Figure 8a shows the SS-SLS of anatase at variable Δλ where the X axis is the emission wavelength λ_{emiss}.

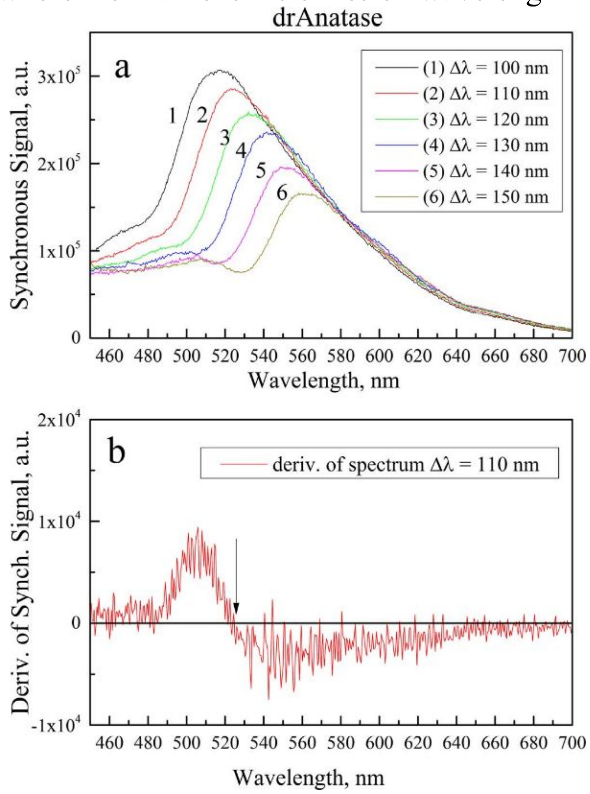

Figure 8. Synchronous luminescence spectra of drAnatase at 25 °C. a) Spectra at variable Δλ. b) The first derivative of spectrum at Δλ = 110 nm.
From Ref. [61]. Reprinted from *Journal of Luminescence*, Vol 192, Alexander Samokhvalov, Trap emission by nanocrystalline anatase in visible range studied by conventional and synchronous luminescence spectroscopy: Adsorption and desorption of water vapor, pages 388-396, Copyright (2017), with permission from Elsevier. License Number 4978280875192.

In Figure 8a, weak shoulder at smaller λ_{emiss} reflects transition across the bandgap. For example, with Δλ = 100 nm, the shoulder at ca. λ_{emiss} = 470 nm corresponds to $\lambda_{exc} = \lambda_{emiss} - \Delta\lambda$ = 470 nm - 100 nm = 370 nm, consistently with E_g of anatase at 3.2 eV or 1240 / 3.2 = 388 nm.

In contrast, the only peak in the derivative SS-SLS in Figure 8b is due to the STE. An example is for Δλ = 110 nm where peak maximum $dS(\lambda_{emiss}) / d\lambda_{emiss} = 0$ is at λ_{emiss} = 524 nm. For the STE peak with λ_{emiss} = 524 nm, the absorption wavelength $\lambda_{exc}(STE) = \lambda_{emiss} - \Delta\lambda$ = 524 nm - 110 nm = 414 nm, which corresponds to energy E(STE) = 1240 / 414 nm = 3.0 eV. Indeed, the STE has the subbandgap transition of lower energy than E_g = 3.2 eV. The ability of the derivative SS-SLS to detect a small difference $\Delta E = E_g - E(STE)$ = 3.2 eV – 3.0 eV = 0.2 eV is a significant advantage.

Further, this is of practical interest to investigate whether numeric values λ_{exc} obtained by the 1-st derivative SS-SLS are "robust" i.e. only slightly depend on choice of Δλ, Table 2. Indeed, when Δλ is varied within 90 nm - 150 nm, the λ_{exc} is only changed from 418 nm to 414 nm. An uncertainty of 4 nm is within the accuracy of most commercial fluorimeters with a single monochromator, and even instruments with dual monochromators, when optical resolution (bandwidth) is set at 5 nm or 10 nm.

Table 2. The wavelengths λ_{exc} to excite the STE in drAnatase determined from synchronous luminescence spectra.

$\Delta\lambda$, nm	The λ_{emiss} at a maximum, nm	The $\lambda_{exc} = \lambda_{emiss} - \Delta\lambda$, nm
90	508	418
100	518	418
110	524	414
120	536	416
130	544	414
140	547	417
150	564	414

From Ref. [61]. Reprinted from *Journal of Luminescence*, Vol 192, Alexander Samokhvalov, Trap emission by nanocrystalline anatase in visible range studied by conventional and synchronous luminescence spectroscopy: Adsorption and desorption of water vapor, pages 388-396, Copyright (2017), with permission from Elsevier. License Number 4978280875192.

Another advantage of the derivative SS-SLS is that a desired λ_{exc} is obtained upon numeric analysis of *just one* spectrum. In contrast, obtaining λ_{exc} from broad "conventional" PL spectra requires (a) the multiple spectra, and (b) a not very reliable numeric multi-peak curve fitting.

An approach of the 1-st derivative SS-SLS was recently utilized [60] to study nanocrystalline rutile TiO_2 at 25 °C. Rutile has absorption and emission of light by free exciton, which is quantum quasi-particle delocalized outside of lattice unit of nanocrystal, in contrast to STE in anatase. In the 1-st derivative SS-SLS of rutile, the $\Delta\lambda$ represents the Stokes shift i.e. the best match between the wavelengths of absorption and emission, and $\Delta\lambda = 180$ nm. The larger $\Delta\lambda$ in rutile than in anatase represents larger loss of energy emitted as a photon by free exciton, consistently with larger delocalization of free exciton versus STE.

To our knowledge, the 2-nd derivative SS-SLS spectra of semiconductors were not reported; this is a promising research direction. Another avenue of interest is the 1-st or 2-nd derivative SS-SLS at the cryogenic temperatures when luminescence intensity is higher. Yet another emerging capability is to study how energy E_g of bandgap (or of other optical transition) is affected upon chemical reaction of solid-state nanomaterial in the "bulk" or on surface.

4.3) Discrimination between surface and "bulk" sites, and studies of surface reactions

Many reactions of solids are accompanied by change in intensity and/or wavelength (energy) of photoluminescence. Nanomaterials feature very high surface area and surface/volume ratio, therefore photoluminescence can be highly sensitive to reactions. The penetration depth of near-UV and visible light through most solid-state materials, including semiconductors is few micrometers. This is significantly larger than the nanocrystal size, so SS-SLS spectra provide a valuable information on electronic states in the "bulk" *and* on surface.

In spectroscopic studies, it is highly desired that only one reactant (or product) is strongly luminescent. In spectroscopic mechanistic studies, water is often used as a "probe molecule", because it has no optical absorption and emission, and thus serves as "dark probe". If luminescence (fluorescence) of a solid is affected by sorption/desorption of water, the SS-SLS aids in identification of active site(s). Observations and conclusions from the SS-SLS are compared to those from "conventional" PL spectra.

One of the benchmark metal-oxide semiconductors is titanium dioxide TiO_2 (titania). It can be present in three crystalline forms: a) anatase; b) rutile and c) a much less abundant brookite [78]. Rutile is the most thermodynamically stable phase of "bulk" TiO_2 and its naturally abundant form. Anatase is more stable than rutile as small nanoparticles [79] which are of significant interest. Namely, nanocrystalline titania containing anatase was studied for sorption in aqueous [80] and non-aqueous [81] media, heterogeneous photocatalysis in aqueous [82] and non-aqueous [83] solutions, and as photocatalyst [84] of gas phase reactions. Other major research interests to nano-anatase and anatase quantum dots [85] are in photovoltaics [86] and specifically solar cells [87], chemo-sensors [88] e.g. humidity sensors [89], in electronic [90] and biomedical [91] devices. Mid-gap states in nano-anatase affect selectivity and yield of photocatalytic reactions and performance of opto-electronic (nano)devices. Mid-gap states were studied by several methods, including steady-state PL spectroscopy [92] and the nanosecond transient infrared absorption spectroscopy [93].

Recently, we reported an SS-SLS study [61] of reversible sorption and desorption of water vapor on nano-anatase in air under ambient conditions. After sorption, visible luminescence is strongly and reversibly decreased ("quenched"), and is increased after water desorption by heating. In the "quenched" sample, "conventional" PL signal is very weak and masked by strong Raman and Rayleigh peaks of adsorbed water, Figure 9a (Raman peaks are "R"). The artifacts dominate in the PL spectra, even when λ_{exc} is systematically varied.

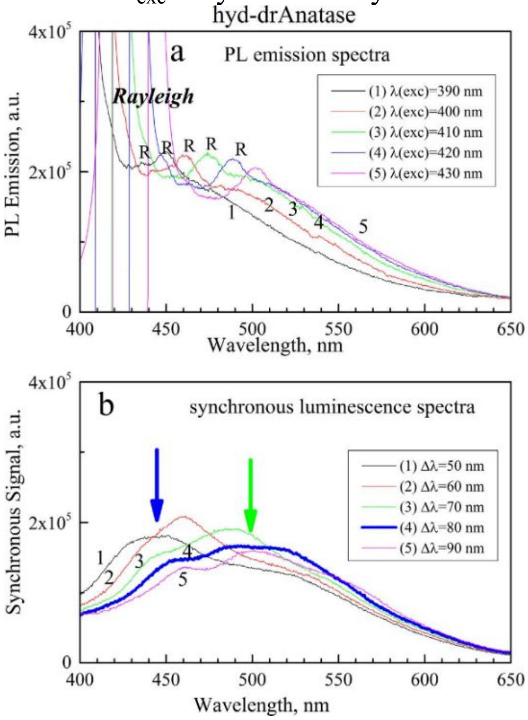

Figure 9. Emission spectra of hyd-drAnatase at 25 °C. a) "Conventional" PL emission spectra. b) Synchronous luminescence spectra.

From Ref. [61]. Reprinted from *Journal of Luminescence*, Vol 192, Alexander Samokhvalov, Trap emission by nanocrystalline anatase in visible range studied by conventional and synchronous luminescence spectroscopy: Adsorption and desorption of water vapor, pages 388-396, Copyright (2017), with permission from Elsevier. License Number 4978280875192.

In contrast, the proper selection of $\Delta\lambda$ in SS-SLS spectra (Figure 9b) allow avoiding both artifacts, and observing three distinct transitions in "hydrated" nano-anatase, despite the strongly quenched emission of light. Luminescence from intrinsic mid-gap state STE at 500 nm is preferentially quenched by water vs. "bulk" charge-trapping states [61] which emit at 450 nm. Further, the SS-SLS with water as "probe molecule" was applied to nanopowders of rutile [60] and strontium titanate [59]. Beyond nanopowders, visible luminescence of micro-crystalline hierarchically structured micro/mesoporous $CaTiO_3$ is strongly decreased (quenched) upon sorption of water, and reversibly increased upon water desorption [58]. The SS-SLS has potential of the quantitative determination of adsorbed water which needs further studies, and may lead to novel optical humidity sensors.

4.4) Studies of composite nanomaterials and mechanisms of heterogeneous reactions

The *in-situ* spectroscopic methods are widely used in mechanistic studies of catalysts [94] and photocatalysts [95]. In "one-pot" photocatalysis with composite nanocrystalline photocatalyst "metal/semiconductor", the latter is *in-situ* photo-synthesized and tested in the same suspension [96, 97]. Recently, we extended applications of SS-SLS to studies of reactions involving composite nanomaterials [54]. The nanocrystalline photocatalyst $Ag(0)/CaTiO_3$ was synthesized by facile "one-pot" photochemically assisted route under UV-visible light, directly in aqueous suspension at 25 °C, and *in-situ* tested for hydrogen generation, Scheme 4.

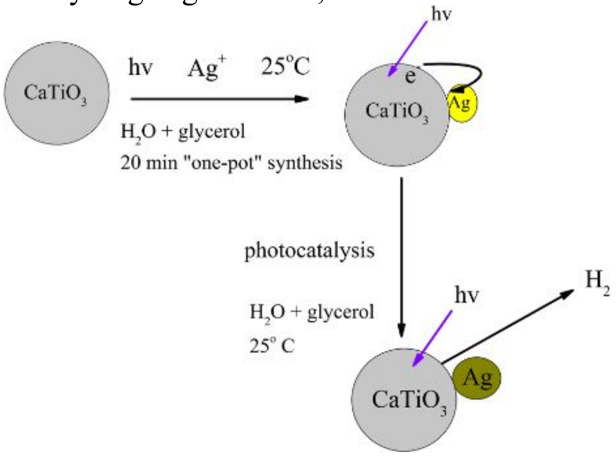

Scheme 4. Scheme of "one-pot" synthesis and in situ photocatalysis with $Ag(0)/CaTiO_3$.
From Ref. [54]. Reprinted with permission from A. Alzahrani, D. Barbash and A. Samokhvalov, "One-pot" synthesis, photocatalytic hydrogen generation with nanocrystalline $Ag(0)/CaTiO_3$ and in-situ mechanistic studies, *J. Phys. Chem. C*, 2016, 120, 19970–19979. Copyright (2016) American Chemical Society.

To observe luminescence from $CaTiO_3$ which emits very weakly [57] at 25 °C but strongly at 77 K, photocatalytic suspension was prepared in a sealed quartz cuvette [54] followed by flash-freezing at 77 K by pouring liquid nitrogen directly on the cuvette. The SS-SLS spectra of flash-frozen suspension reveal strong luminescence quenching osf $CaTiO_3$ in $Ag(0)/CaTiO_3$, Figure 10.

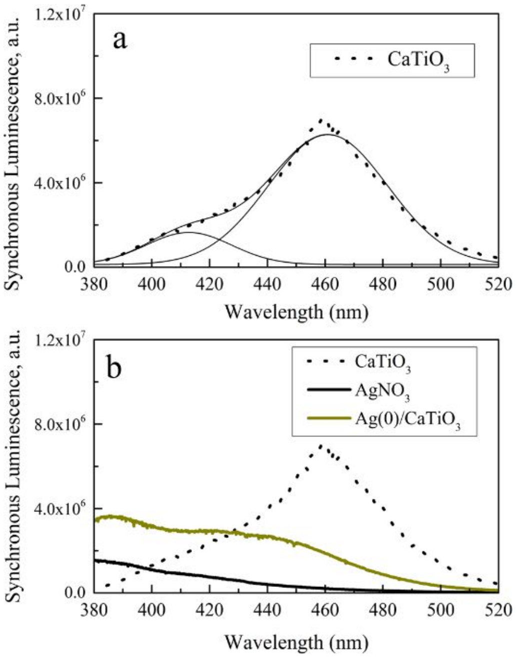

Figure 10. In situ synchronous luminescence spectra in glycerol/water matrix at 77 K after illumination. (a) $CaTiO_3$ with numeric fitting. (b) $CaTiO_3$, $AgNO_3$ precursor, and a mixture of $CaTiO_3$ and $AgNO_3$.

From Ref. [54]. Reprinted with permission from A. Alzahrani, D. Barbash and A. Samokhvalov, "One-pot" synthesis, photocatalytic hydrogen generation with nanocrystalline Ag(0)/$CaTiO_3$ and in-situ mechanistic studies, *J. Phys. Chem. C*, 2016, 120, 19970–19979. Copyright (2016) American Chemical Society.

PL quenching is due to bonding of $CaTiO_3$ nanocrystals to metallic Ag(0) NPs, and transfer of photoexcited electron from the CB of $CaTiO_3$ to electronic states of metal, Scheme 5.

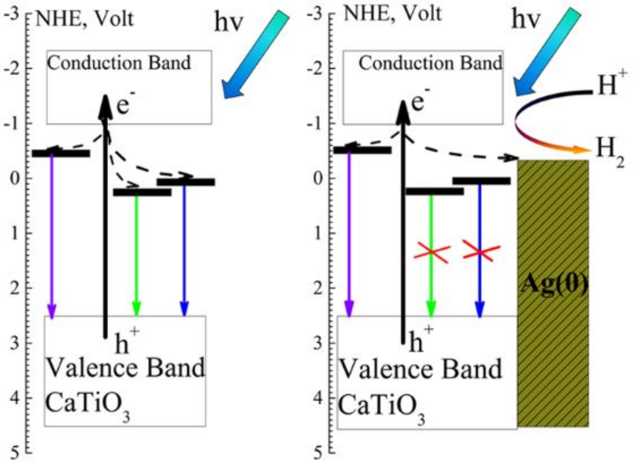

Scheme 5. Energy diagram for relaxation of photoexcited charge. (a) $CaTiO_3$. (b) Ag(0)/$CaTiO_3$ photocatalyst.

From Ref. [54]. Reprinted with permission from A. Alzahrani, D. Barbash and A. Samokhvalov, "One-pot" synthesis, photocatalytic hydrogen generation with nanocrystalline Ag(0)/$CaTiO_3$ and in-situ mechanistic studies, *J. Phys. Chem. C*, 2016, 120, 19970–19979. Copyright (2016) American Chemical Society.

In experiment in ref. [54], the specimen had to be removed from the photocatalytic reactor and inserted to the sample compartment of fluorescence spectrometer. In contrast, *in-situ* spectra track progress of reaction with specimen in the sample compartment. The *in-situ* spectroscopy has been developed for studies of heterogeneous catalysis [98] and applied to mechanistic studies of sorption [99]. The Operando approach is a "combination of *in-situ* spectroscopy and simultaneous activity measurements under catalytic reaction conditions" [100]. The Operando is not limited by catalysis, and it has been utilized in studies of sorption [101, 102]. In our opinion, *in-situ* and Operando SS-SLS has strong potential to contribute to studies of kinetics and mechanism of consumption of reactants in reactions "solid/liquid", selective monitoring of formation and consumption of solid-state nanomaterials, and their quantitative analysis. Importantly, the SS-SLS has potential in kinetic studies of solid-state materials as their reactions are often slow, with half-times much larger than the typical scanning time of optical monochromators in the fluorescence spectrometer.

5) Outlook, challenges and opportunities

The SS-SLS is a novel, powerful, high-resolution method of studies of nanocrystalline semiconductors and their reactions. In our opinion, SS-SLS has the significant potential in studies of semiconductors and insulators beyond metal oxides, and beyond studies of sorption. In industry, PL spectroscopy finds use in quality control of devices and films with hetero-structures including silicon and other major materials e.g. gallium nitride [103]. Imaging based on "conventional" PL spectra is a routine tool of quality control in manufacturing silicon wafers [104]. The opportunities of the SS-SLS beyond research lab are where PL spectra and imaging are used, but with a significantly improved resolution. Certain metal oxides studied by SS-SLS [57-61] are minerals used as pigments. The SS-SLS is capable of accurate determination of energy of absorption and emission of light, so spectra of characteristic impurities can be used in forensic analysis. Another avenue is the quantitative SS-SLS for detection of the amount of adsorbate based on luminescence quenching, which could find use in optical humidity and other sensors.

In applied surface science, the SS-SLS can be used for accurate characterization of dopants in semiconductors and insulators. An exciting opportunity is detection of metal-induced gap states (MIGS) at semiconductor/metal junction [105] of moderate- to wide-bandgap semiconductors, as these studies can be facilely conducted in visible range without costly upgrades to the NIR optics. For optoelectronics, a moderately large penetration depth of near-UV and visible light at few micrometers would allow depth profiling, which is promising for determination of band gaps of nanomaterials in sandwich-like quantum devices e.g. light-emitting diodes [106] and staggered gap quantum wells [107]. Studies of 2D materials such as MoS_2 by PL [108] are very common and are of significant interest. However, "conventional" PL spectra of such materials are quite wide and often have structured shoulders, e.g. spectra of MoS_2 nanoflakes with and without Au support in ref. [109]. Spectral shoulders A1 and B1 in Figure 2 in ref. [109] are due to exciton peaks, which are not included in energy band diagram and their accurate energy cannot be determined. The SS-SLS would have the significantly narrowed peaks with well-defined maxima, so that these excitonic states can be included and the energy diagram completed. Plasmon-enhanced fluorescence from metal-semiconductor nanostructures [110] can be better resolved using SS-SLS and contributions by interfacial states to plasmonic phenomena can be understood. The contemporary instrumental science can benefit from developing the second derivative SS-SLS, which was not yet reported for inorganic compounds. The potential indirect cost advantages of the SS-SLS vs. "conventional" PL spectroscopy include the more comprehensive analysis by the single method, thus avoiding use of the complementary instruments which may be expensive, such as UPS etc.

Yet another possibility is *in-situ* and Operando SS-SLS where studies of sorption and catalysis of gases are straightforward. On the other hand, adapting *in-situ* SS-SLS for studies of suspensions is challenging due to optical scattering, but potentially rewarding due to the large number of industrial processes involving liquids. We believe that an enhanced-resolution, facile, non-contact and non-destructive instrumental method of solid-state synchronous luminescence spectroscopy has significant potential to contribute to solid-state, inorganic and coordination chemistry, catalysis and photocatalysis, sensing, optoelectronic materials and devices, and more in the years to come.

Acknowledgement

Research was sponsored by the Army Research Office and was accomplished under Grant Number **W911NF-20-1-0290**. The views and conclusions contained in this document are those of the authors and should not be interpreted as representing the official policies, either expressed or implied, of the Army Research Office or the U.S. Government. The U.S. Government is authorized to reproduce and distribute reprints for Government purposes notwithstanding any copyright notation herein.

References

[1] T.O. Wehling, M.I. Katsnelson and A.I. Lichtenstein, Impurities on graphene: Midgap states and migration barriers, *Phys. Rev. B*, 2009, **80**, 085428.

[2] P.T.T. Le, K. Mirabbaszadeh, M. Davoudiniya and M. Yarmohammadi, Charged impurity-tuning of midgap states in biased Bernal bilayer black phosphorus: An anisotropic electronic phase transition, *Phys. Chem. Chem. Phys.*, 2018, **20**, 25044-25051.

[3] J.A. Luceño-Sánchez, A.M. Díez-Pascual and R. Peña Capilla, Materials for photovoltaics: State of art and recent developments, *Int. J. Mol. Sci.*, 2019, **20**, 976.

[4] K. Konstantinou, F.C. Mocanu, T.-H. Lee and S.R. Elliott, Revealing the intrinsic nature of the mid-gap defects in amorphous $Ge_2Sb_2Te_5$, *Nat. Commun.*, 2019, **10**, 3065.

[5] H. Jin, E. Debroye, M. Keshavarz, I.G. Scheblykin, M.B.J. Roeffaers, J. Hofkens and J.A. Steele, It's a trap! On the nature of localised states and charge trapping in lead halide perovskites, *Mater. Horizons*, 2020, **7**, 397-410.

[6] H. Yaghoubi, Z. Li, Y. Chen, H.T. Ngo, V.R. Bhethanabotla, B. Joseph, S. Ma, R. Schlaf and A. Takshi, Toward a visible light-driven photocatalyst: The effect of midgap-states-induced energy gap of undoped TiO_2 nanoparticles, *ACS Catal.*, 2015, **5**, 327-335.

[7] C. Maheu, L. Cardenas, E. Puzenat, P. Afanasiev and C. Geantet, UPS and UV spectroscopies combined to position the energy levels of TiO_2 anatase and rutile nanopowders, *Phys. Chem. Chem. Phys.*, 2018, **20**, 25629-25637.

[8] C.-P. Lu, G. Li, J. Mao, L.-M. Wang and E.Y. Andrei, Bandgap, mid-gap states, and gating effects in MoS_2, *Nano Lett.*, 2014, **14**, 4628-4633.

[9] A. Gloter, C. Ewels, P. Umek, D. Arcon and C. Colliex, Electronic structure of titania-based nanotubes investigated by EELS spectroscopy, *Phys. Rev. B*, 2009, **80**, 035413.

[10] D. Hauschild, E. Handick, S. Göhl-Gusenleitner, F. Meyer, H. Schwab, A. Benkert, S. Pohlner, J. Palm, S. Tougaard, C. Heske, L. Weinhardt and F. Reinert, Band-gap widening at the $Cu(In,Ga)(S,Se)_2$ surface: A novel determination approach using reflection electron energy loss spectroscopy, *ACS. Appl. Mater. Interfaces*, 2016, **8**, 21101-21105.

[11] E. Liberti, R. Menzel, M.S.P. Shaffer and D.W. McComb, Probing the size dependence on the optical modes of anatase nanoplatelets using STEM-EELS, *Nanoscale*, 2016, **8**, 9727-9735.

[12] A. Gloter, A. Douiri, M. Tencé and C. Colliex, Improving energy resolution of EELS spectra: An alternative to the monochromator solution, *Ultramicroscopy*, 2003, **96**, 385-400.

[13] O.L. Krivanek, N. Dellby, J.A. Hachtel, J.C. Idrobo, M.T. Hotz, B. Plotkin-Swing, N.J. Bacon, A.L. Bleloch, G.J. Corbin, M.V. Hoffman, C.E. Meyer and T.C. Lovejoy, Progress in ultrahigh energy resolution EELS, *Ultramicroscopy*, 2019, **203**, 60-67.

[14] I. Abdallah, C. Dupressoire, L. Laffont, D. Monceau and A. Vande Put, STEM-EELS identification of TiO_xN_y, TiN, Ti_2N and O, N dissolution in the Ti2642S alloy oxidized in synthetic air at 650 °C, *Corros. Sci.*, 2019, **153**, 191-199.

[15] L. Tao and A. Khursheed, Transmission EELS attachment for SEM, *IEEE Trans. Device Mater. Reliab.*, 2006, **6**, 182-185.

[16] R.F. Egerton, Scattering delocalization and radiation damage in STEM-EELS, *Ultramicroscopy*, 2017, **180**, 115-124.

[17] F.R. Trouw and D.L. Price, Chemical applications of neutron scattering, *Annu. Rev. Phys. Chem.*, 1999, **50**, 571-601.

[18] H. Kanzaki, S. Sakuragi, S. Hoshino, G. Shirane and Y. Fujii, Neutron scattering study of phonons associated with indirect band-gap transition in AgBr, *Solid State Commun.*, 1974, **15**, 1547-1550.

[19] S. Paul and A. Choudhury, Investigation of the optical property and photocatalytic activity of mixed phase nanocrystalline titania, *Appl. Nanosci.*, 2014, **4**, 839-847.

[20] H.G. Hecht, The interpretation of diffuse reflectance spectra, *J. Res. Natl. Bur. Stand. A Phys. Chem.*, 1976, **80A**, 567-583.

[21] D.L. Wood and J. Tauc, Weak absorption tails in amorphous semiconductors, *Phys. Rev. B*, 1972, **5**, 3144-3151.

[22] J.B.M. Goodall, S. Kellici, D. Illsley, R. Lines, J.C. Knowles and J.A. Darr, Optical and photocatalytic behaviours of nanoparticles in the Ti–Zn–O binary system, *RSC Adv.*, 2014, **4**, 31799-31809.

[23] G.D. Cody, Urbach edge of crystalline and amorphous silicon: A personal review, *J. Non Cryst. Solids*, 1992, **141**, 3-15.

[24] H. Tang, F. Lévy, H. Berger and P.E. Schmid, Urbach tail of anatase TiO_2, *Phys. Rev. B*, 1995, **52**, 7771-7774.

[25] C.H. Seager, P.M. Lenahan, K.L. Brower and R.E. Mikawa, Dangling bonds and the Urbach tail in silicon, *J. Appl. Phys.*, 1985, **58**, 2704-2708.

[26] P.P.T. Chen, K.S.A. Butcher, E.M. Goldys, T.L. Tansley and K.E. Prince, High energy Urbach characteristic observed for gallium nitride amorphous surface oxide, *Thin Solid Films*, 2006, **496**, 342-345.

[27] J. Chantana, Y. Kawano, T. Nishimura, A. Mavlonov and T. Minemoto, Impact of Urbach energy on open-circuit voltage deficit of thin-film solar cells, *Sol. Energy Mater Sol.*, 2020, **210**, 110502.

[28] V.R. Akshay, B. Arun, G. Mandal and M. Vasundhara, Visible range optical absorption, urbach energy estimation and paramagnetic response in Cr-doped TiO_2 nanocrystals derived by a sol–gel method, *Phys. Chem. Chem. Phys.*, 2019, **21**, 12991-13004.

[29] G.D. Gilliland, Photoluminescence spectroscopy of crystalline semiconductors, *Mater. Sci. Eng. R Rep.*, 1997, **18**, 99-399.

[30] P.J. Ventura, M.F. Cerqueira, M.C. Carmo and J.A. Ferreira, Photoluminescence and structure properties from μc-Si:H and μc-Si:H-PS samples, *Thin Solid Films*, 1997, **296**, 126-128.

[31] L.A. Aslanov, V.B. Zaytsev, V.N. Zakharov, I.K. Kudryavtsev, V.M. Senyavin, P.B. Lagov and Y.S. Pavlov, Nanosilicon stabilized with ligands: Effect of high-energy electron beam on luminescent properties, *Surf. Interface Anal.*, 2020, **52**, 957-961.

[32] K.V. Reich, T. Chen, A.L. Efros and B.I. Shklovskii, Photoluminescence in array of doped semiconductor nanocrystals, *Phys. Rev. B*, 2013, **88**, 245311

[33] C.P. Saini, A. Barman, D. Banerjee, O. Grynko, S. Prucnal, M. Gupta, D.M. Phase, A.K. Sinha, D. Kanjilal, W. Skorupa and A. Kanjilal, Impact of self-trapped excitons on blue photoluminescence in TiO_2 nanorods on chemically etched Si pyramids, *J. Phys. Chem. C*, 2017, **121**, 11448-11454.

[34] O. Auciello and D.M. Aslam, Review on advances in microcrystalline, nanocrystalline and ultrananocrystalline diamond films-based micro/nano-electromechanical systems technologies, *J. Mater. Sci.*, 2021, **56**, 7171-7230.

[35] Y. Chen, P. Lu, Q. Gui, Z. Li, Y. Yuan and H. Zhang, Preparation of chiral luminescent liquid crystals and manipulation effect of phase structures on the circularly polarized luminescence property, *J. Mater. Chem C*, 2021, **9**, 1279-1286.

[36] J.R. Lakowicz, Principles of fluorescence spectroscopy, 3rd ed., Springer, New York, 2006.

[37] P.-A. Cazade, P. Bordat, S. Blanc, I. Baraille and R. Brown, Possible artifacts of fluorescence of dyes in concentrated materials: Comment on “Highly fluorescent Rhodamine B nanoparticles entrapped in hybrid glasses”, *Langmuir*, 2008, **24**, 2252-2257.
[38] T. Larsson, M. Wedborg and D. Turner, Correction of inner-filter effect in fluorescence excitation-emission matrix spectrometry using Raman scatter, *Anal. Chim. Acta*, 2007, **583**, 357-363.
[39] T. Wang, L.-H. Zeng and D.-L. Li, A review on the methods for correcting the fluorescence inner-filter effect of fluorescence spectrum, *Appl. Spectrosc. Rev.*, 2017, **52**, 883-908.
[40] H. Pan, H. Yu, Y. Wang, R. Liu and H. Lei, Investigating variations of fluorescent dissolved organic matter in wastewater treatment using synchronous fluorescence spectroscopy combined with principal component analysis and two-dimensional correlation, *Environ. Technol.*, 2018, **39**, 2495-2502.
[41] A. Sahar, T. Boubellouta, J. Lepetit and É. Dufour, Front-face fluorescence spectroscopy as a tool to classify seven bovine muscles according to their chemical and rheological characteristics, *Meat Science*, 2009, **83**, 672-677.
[42] V. Dalal, R. Knox and B. Moradi, Measurement of Urbach edge and midgap states in amorphous silicon p-i-n devices, *Sol. Energy Mater. Sol. Cells*, 1993, **31**, 349-356.
[43] A. Kahn, Fermi level, work function and vacuum level, *Mater. Horiz.*, 2016, **3**, 7-10.
[44] P. Nagpal and V.I. Klimov, Role of mid-gap states in charge transport and photoconductivity in semiconductor nanocrystal films, *Nat. Commun.*, 2011, **2**, 486.
[45] A. Krause, W. Weber, A. Jahn, K. Richter, D. Pohl, B. Rellinghaus, U. Schröder, J. Heitmann and T. Mikolajick, Evaluation of the electrical and physical properties of thin calcium titanate high-k insulators for capacitor applications, *J. Vac. Sci. Technol., B*, 2011, **29**, 01AC07.
[46] J. Gerblinger and H. Meixner, Fast oxygen sensors based on sputtered strontium titanate, *Sensor. Actuat. B-Chem*, 1991, **4**, 99-102.
[47] P. Sánchez and A. Stashans, Computational study of structural and electronic properties of superconducting La-doped $SrTiO_3$, *Philos. Mag. B*, 2001, **81**, 1963-1976.
[48] D. Zhang, M. Wang, G.J. Ren and E.J. Song, Preparation of biomorphic porous calcium titanate and its application for preconcentration of nickel in water and food samples, *Mater. Sci. Eng. C Mater. Biol. Appl.*, 2013, **33**, 4677-4683.
[49] K. Hbaieb, Exploring strontium titanate as a reforming catalyst for dodecane, *Appl. Nanosci.*, 2016, **6**, 847-854.
[50] W. Wang, M.O. Tadé and Z. Shao, Research progress of perovskite materials in photocatalysis- and photovoltaics-related energy conversion and environmental treatment, *Chem. Soc. Rev.*, 2015, **44**, 5371-5408.
[51] Y. Xu and M.A.A. Schoonen, The absolute energy positions of conduction and valence bands of selected semiconducting minerals, *Am. Mineral.*, 2000, **85**, 543-556.
[52] H. Yoshida, L. Zhang, M. Sato, T. Morikawa, T. Kajino, T. Sekito, S. Matsumoto and H. Hirata, Calcium titanate photocatalyst prepared by a flux method for reduction of carbon dioxide with water, *Catal. Today*, 2015, **251**, 132-139.
[53] S. Liu, Y. Qu, R. Li, G. Wang and Y. Li, Photocatalytic activity of $MTiO_3$ (M = Ca, Ni, and Zn) nanocrystals for water decomposition to hydrogen, *J. Mater. Res.*, 2014, **29**, 1295-1301.
[54] A. Alzahrani, D. Barbash and A. Samokhvalov, “One-pot” synthesis and photocatalytic hydrogen generation with nanocrystalline Ag(0)/$CaTiO_3$ and in situ mechanistic studies, *J. Phys. Chem. C*, 2016, **120**, 19970–19979.

[55] A.M. Ferrari, T.O. Germiniano, J.E. Savoia, R.G. Marques, V.A.d.S. Ribeiro and A.C. Ueda, $CaTiO_3$ perovskite in the photocatalysis of textile wastewater, *Revista Ambiente & Água*, 2019, **14**.

[56] P. Kanhere and Z. Chen, A review on visible light active perovskite-based photocatalysts, *Molecules*, 2014, **19**, 19995-20022.

[57] A. Alzahrani and A. Samokhvalov, Conventional and cryo-synchronous luminescence spectra of orthorhombic calcium titanate, *J. Lumin.*, 2016, **178**, 430-436.

[58] A. Alzahrani and A. Samokhvalov, Porous calcium titanate and sorption and desorption of water under ambient conditions: A study by conventional and synchronous luminescence spectroscopy, *J. Porous Mater.*, 2017, **24**, 1145-1154.

[59] S. Taylor and A. Samokhvalov, Water as probe molecule for midgap states in nanocrystalline strontium titanate by conventional and synchronous luminescence spectroscopy under ambient conditions, *Spectrochim. Acta A*, 2017, **174**, 54-61.

[60] A. Samokhvalov, Visible emission in nanocrystalline rutile: Free exciton and water as probes for midgap states in adsorption/desorption using "conventional" and synchronous luminescence spectroscopy, *J. Phys. Chem. C*, 2017, **121**, 21985-21994.

[61] A. Samokhvalov, Trap emission by nanocrystalline anatase in visible range studied by conventional and synchronous luminescence spectroscopy: Adsorption and desorption of water vapor, *J. Lumin.*, 2017, **192**, 388-396.

[62] G.L. Green and T.C. O'Haver, Derivative luminescence spectrometry, *Anal. Chem.*, 1974, **46**, 2191-2196.

[63] Y.A. Salem, M.E.A. Hammouda, M.A. Abu El-Enin and S.M. El-Ashry, Application of derivative emission fluorescence spectroscopy for determination of ibuprofen and phenylephrine simultaneously in tablets and biological fluids, *Spectrochim. Acta A Mol. Biomol. Spectrosc.*, 2019, **210**, 387-397.

[64] F.G. Sanchez and C.C. Blanco, Synchronous derivative room-temperature phosphorescence determination of warfarin in blood serum, *Anal. Chim. Acta*, 1989, **222**, 177-188.

[65] T.C. O'Haver, A.F. Fell, G. Smith, P. Gans, J. Sneddon, L. Bezur, R.G. Michel, J.M. Ottaway, J.N. Miller, T.A. Ahmad, A.F. Fell, B.P. Chadburn and C.T. Cottrell, Derivative spectroscopy and its applications in analysis, *Anal. Proc.*, 1982, **19**, 22-46.

[66] J. Xi, Q. Zhang, D. Myers, G. Cao and Y. Sun, Hollow hemispherical titanium dioxide aggregates fabricated by coaxial electrospray for dye-sensitized solar cell application, *J. Nanophotonics*, 2012, **6**, 063519.

[67] X. Yao, H. Jin, C. Liu and S.S.C. Chuang, 5 - TiO_2-based photocatalytic conversion processes: Insights from in situ infrared spectroscopy, in: X. Wang, M. Anpo, X. Fu (Eds.) Current developments in photocatalysis and photocatalytic materials, Elsevier, 2020, pp. 57-75.

[68] S. Livraghi, M.R. Chierotti, E. Giamello, G. Magnacca, M.C. Paganini, G. Cappelletti and C.L. Bianchi, Nitrogen-doped titanium dioxide active in photocatalytic reactions with visible light: A multi-technique characterization of differently prepared materials, *J. Phys. Chem. C*, 2008, **112**, 17244-17252.

[69] M. Iwasaki, M. Hara, H. Kawada, H. Tada and S. Ito, Cobalt ion-doped TiO_2 photocatalyst response to visible light, *J. Colloid Interface Sci.*, 2000, **224**, 202-204.

[70] T. Sun, J. Fan, E.Z. Liu, L.S. Liu, Y. Wang, H.Z. Dai, Y.H. Yang, W.Q. Hou, X.Y. Hu and Z.Y. Jiang, Fe and Ni co-doped TiO_2 nanoparticles prepared by alcohol-thermal method: Application in hydrogen evolution by water splitting under visible light irradiation, *Powder Technol.*, 2012, **228**, 210-218.

[71] T. Tachikawa, S. Tojo, K. Kawai, M. Endo, M. Fujitsuka, T. Ohno, K. Nishijima, Z. Miyamoto and T. Majima, Photocatalytic oxidation reactivity of holes in the sulfur- and carbon-doped TiO_2 powders studied by time-resolved diffuse reflectance spectroscopy, *J. Phys. Chem. B*, 2004, **108**, 19299-19306.

[72] A. Samokhvalov, Hydrogen by photocatalysis with nitrogen codoped titanium dioxide, *Renew. Sust. Energ. Rev*, 2017, **72**, 981-1000.

[73] X. Chen, L. Liu and F. Huang, Black titanium dioxide (TiO_2) nanomaterials, *Chem. Soc. Rev.*, 2015, **44**, 1861-1885.

[74] A.V. Emeline, V.N. Kuznetsov, V.K. Rybchuk and N. Serpone, Visible-light-active titania photocatalysts: The case of N-doped TiO_2S - properties and some fundamental issues, *Int. J. Photoenergy*, 2008, **2008**, 258394.

[75] A. Stevanovic, M. Büttner, Z. Zhang and J.T. Yates, Photoluminescence of TiO_2: Effect of UV light and adsorbed molecules on surface band structure, *J. Am. Chem. Soc.*, 2012, **134**, 324-332.

[76] I. Sildos, A. Suisalu, J. Aarik, T. Sekiya and S. Kurita, Self-trapped exciton emission in crystalline anatase, *J. Lumin.*, 2000, **87-89**, 290-292.

[77] L. Cavigli, F. Bogani, A. Vinattieri, L. Cortese, M. Colocci, V. Faso and G. Baldi, Carrier recombination dynamics in anatase TiO_2 nanoparticles, *Solid State Sci.*, 2010, **12**, 1877-1880.

[78] D. D'Elia, C. Beauger, J.F. Hochepied, A. Rigacci, M.H. Berger, N. Keller, V. Keller-Spitzer, Y. Suzuki, J.C. Valmalette, M. Benabdesselam and P. Achard, Impact of three different TiO_2 morphologies on hydrogen evolution by methanol assisted water splitting: Nanoparticles, nanotubes and aerogels, *Int. J. Hydrog. Energy*, 2011, **36**, 14360-14373.

[79] M.R. Ranade, A. Navrotsky, H.Z. Zhang, J.F. Banfield, S.H. Elder, A. Zaban, P.H. Borse, S.K. Kulkarni, G.S. Doran and H.J. Whitfield, Energetics of nanocrystalline TiO_2, *Proc. Natl. Acad. Sci USA*, 2002, **99**, 6476-6481.

[80] P.J. Holliman, B. Vaca Velasco, I. Butler, M. Wijdekop and D.A. Worsley, Studies of dye sensitisation kinetics and sorption isotherms of Direct Red 23 on titania, *Int. J. Photoenergy*, 2008, **2008**, 827605.

[81] A. Samokhvalov, S. Nair, E.C. Duin and B.J. Tatarchuk, Surface characterization of Ag/Titania adsorbents, *Appl. Surf. Sci.*, 2010, **256**, 3647-3652.

[82] R. Ramakrishnan, S. Kalaivani, J.A.I. Joice and T. Sivakumar, Photocatalytic activity of multielement doped TiO_2 in the degradation of Congo Red, *Appl. Surf. Sci.*, 2012, **258**, 2515-2521.

[83] M. Zielinski , L.A. Burke and A. Samokhvalov, Selective activation of C=C bond in sustainable phenolic compounds from lignin via photooxidation: Experiment and density functional theory calculations, *Photochem. Photobiol.*, 2015, **91**, 1332-1339.

[84] C. Ampelli, R. Passalacqua, C. Genovese, S. Perathoner, G. Centi, T. Montini, V. Gombac, J.J. Delgado Jaen and P. Fornasiero, H_2 production by selective photo-dehydrogenation of ethanol in gas and liquid phase on CuO_x/TiO_2 nanocomposites, *RSC Adv.*, 2013, **3**, 21776-21788.

[85] L. Gnanasekaran, R. Hemamalini and K. Ravichandran, Synthesis and characterization of TiO_2 quantum dots for photocatalytic application, *J. Saudi Chem. Soc.*, 2015, **19**, 589-594.

[86] Y. Bai, I. Mora-Seró, F. De Angelis, J. Bisquert and P. Wang, Titanium dioxide nanomaterials for photovoltaic applications, *Chem. Rev.*, 2014, **114**, 10095-10130.

[87] B. Tan and Y. Wu, Dye-sensitized solar cells based on anatase TiO_2 nanoparticle/nanowire composites, *J. Phys. Chem. B*, 2006, **110**, 15932-15938.

[88] N.O. Savage, B. Chwieroth, A.S. Ginwalla, B. Patton, S.A. Akbar and P. Dutta, Composite n-p semiconducting titanium oxides as gas sensors, *Sens. Actuator B-Chem*, 2001, **79**, 17-27.
[89] M. Ghadiry, M. Gholami, L.C. Kong, C.W. Yi, H. Ahmad and Y. Alias, Nano-anatase TiO_2 for high performance optical humidity sensing on chip, *Sensors*, 2015, **16**, 39.
[90] A. Tamilselvan and S. Balakumar, Anatase TiO_2 nanotube by electrochemical anodization method: Effect of tubes dimension on the supercapacitor application, *Ionics*, 2016, **22**, 99-105.
[91] L. Visai, L. De Nardo, C. Punta, L. Melone, A. Cigada, M. Imbriani and C.R. Arciola, Titanium oxide antibacterial surfaces in biomedical devices, *Int. J. Artif. Organs*, 2011, **34**, 929-946.
[92] D.K. Pallotti, L. Passoni, P. Maddalena, F. Di Fonzo and S. Lettieri, Photoluminescence mechanisms in anatase and rutile TiO_2, *J. Phys. Chem. C*, 2017, **121**, 9011-9021.
[93] M. Zhu, Y. Mi, G. Zhu, D. Li, Y. Wang and Y. Weng, Determination of midgap state energy levels of an anatase TiO_2 nanocrystal film by nanosecond transient infrared absorption – excitation energy scanning spectra, *J. Phys. Chem. C*, 2013, **117**, 18863-18869.
[94] J. King, C. Liu and S.S.C. Chuang, In situ infrared approach to unravel reaction intermediates and pathways on catalyst surfaces, *Res. Chem. Intermed.*, 2019, **45**, 5831-5847.
[95] J. Tan, L. Yang, Q. Kang and Q. Cai, In situ ATR-FTIR and UV-Visible spectroscopy study of photocatalytic oxidation of ethanol over TiO_2 nanotubes, *Anal. Lett.*, 2011, **44**, 1114-1125.
[96] M. Mehta, S. Taylor and A. Samokhvalov, Photochemical synthesis, characterization, photoinduced electron transfer, charging and discharging in copper-titania colloid, *J. Photochem. Photobiol., A*, 2016, **317**, 1-8.
[97] Y.-H. Chung, K. Han, C.-Y. Lin, D. O'Neill, G. Mul, B. Mei and C.-M. Yang, Photocatalytic hydrogen production by photo-reforming of methanol with one-pot synthesized Pt-containing TiO_2 photocatalysts, *Catal. Today*, 2020, **356**, 95-100.
[98] M. Hunger and J. Weitkamp, In situ IR, NMR, EPR, and UV/Vis spectroscopy: Tools for new insight into the mechanisms of heterogeneous catalysis, *Angew. Chem. Int. Ed.*, 2001, **40**, 2954-2971.
[99] A. Samokhvalov, E.C. Duin, S. Nair and B.J. Tatarchuk, An in situ temperature-programmed XPS study of the surface chemical reactions of thiophene with Ag/Titania, *Surf. Interface Anal.*, 2010, **42**, 1476–1482.
[100] M.A. Banares, Operando methodology: Combination of in situ spectroscopy and simultaneous activity measurements under catalytic reaction conditions, *Catal. Today*, 2005, **100**, 71-77.
[101] A. Samokhvalov and B.J. Tatarchuk, Characterization of active sites, determination of mechanisms of H_2S, COS and CS_2 sorption and regeneration of ZnO low-temperature sorbents: Past, current and perspectives, *Phys. Chem. Chem. Phys.*, 2011, **13**, 3197-3209.
[102] P. Dhage, A. Samokhvalov, D. Repala, E.C. Duin and B.J. Tatarchuk, Regenerable Fe-Mn-ZnO/SiO_2 sorbents for room temperature removal of H_2S from fuel reformates: Performance, active sites, Operando studies, *Phys. Chem. Chem. Phys.*. 2011, **13**, 2179-2187.
[103] G. Santana, O. De Melo, J. Aguilar-Hernández, R. Mendoza-Pérez, B.M. Monroy, A. Escamilla-Esquivel, M. López-López, F. De Moure, L.A. Hernández and G. Contreras-Puente, Photoluminescence study of gallium nitride thin films obtained by infrared close space vapor transport, *Materials*, 2013, **6**, 1050-1060.
[104] J. Haunschild, M. Glatthaar, M. Demant, J. Nievendick, M. Motzko, S. Rein and E.R. Weber, Quality control of as-cut multicrystalline silicon wafers using photoluminescence imaging for solar cell production, *Sol. Energy Mater. Sol. Cells*, 2010, **94**, 2007-2012.

[105] G.-S. Kim, S.-H. Kim, J. Park, K.H. Han, J. Kim and H.-Y. Yu, Schottky barrier height engineering for electrical contacts of multilayered MoS_2 transistors with reduction of metal-induced gap states, *ACS Nano*, 2018, **12**, 6292-6300.

[106] A. Gorai, S. Panda and D. Biswas, Advantages of InGaN/InGaN quantum well light emitting diodes: Better electron-hole overlap and stable output, *Optik*, 2017, **140**, 665-672.

[107] K. Louarn, Y. Claveau, L. Marigo-Lombart, C. Fontaine, A. Arnoult, F. Piquemal, A. Bounouh, N. Cavassilas and G. Almuneau, Effect of low and staggered gap quantum wells inserted in gaas tunnel junctions, *J. Phys. D Appl. Phys.*, 2018, **51**, 145107.

[108] Y. Liu, S. Wang, X. Chen, M. Yang, X. Li and B. Liang, Folded MoS_2 bilayers with variable interfacial coupling revealed by Raman and photoluminescence spectroscopy, *Opt. Mater.*, 2021, **111**, 110641.

[109] U. Bhanu, M.R. Islam, L. Tetard and S.I. Khondaker, Photoluminescence quenching in gold - MoS_2 hybrid nanoflakes, *Sci. Rep.*, 2014, **4**, 5575.

[110] H. Naiki, A. Masuhara, S. Masuo, T. Onodera, H. Kasai and H. Oikawa, Highly controlled plasmonic emission enhancement from metal-semiconductor quantum dot complex nanostructures, *J. Phys. Chem. C*, 2013, **117**, 2455-2459.